Chapter 3

Results

3.1 AKAP7δ-derived peptides bind RII subunits with high affinity

Compartmentalisation of PKA, PKA substrates and regulators of PKA function is achieved by AKAPs. The role of compartmentalisation for cellular function is studied by dislocation of such complexes or displacement of selected protein components from such complexes. AKAPs bind PKA *via* a structurally conserved amphipathic helix. Hydrophobic amino acid residues in conserved positions mediate binding to the dimer of R subunits of the PKA. AKAPs are diverse in their targeting and recruitment of signalling proteins (see 1.3). Uncoupling of the PKA from AKAP is the crucial step for the investigation of compartmentalisation of PKA. Uncoupling is achievable with peptides that mimic the RII-binding domain of AKAPs and competitively inhibit the interaction with RII subunits. (see 1.4).

The observation that truncated AKAP7δ binds RII subunits with higher affinity than the full length protein and the fact that AKAP7δ is one of the AKAPs with the highest affinity to RII subunits [71], led to the idea to de-

velop peptides derived from the RII-binding domain of AKAP7δ as putative disruptors of PKA anchoring. Peptides comprising 25 amino acids (25-mer; position 296-320) of AKAP7δ corresponding to the RII-binding domain were used as basis. The wild-type sequence of this 25-mer was substituted in each position by any of the 20 biogenous amino acids and spot-synthesised on a cellulose membrane (peptide substitution array). The membrane was assayed by RII overlay with a mix of bovine RIIα and RIIβ subunits. The autoradiography of the membrane (Fig. 3.1) displays high affinity binding for most of the spots (dark spots). The substitution by cysteine led to unreproducible results as cysteine forms disulphide bonds under the oxidative conditions of synthesis and was therefore excluded from all further experiments based on spot-synthesis. Hydrophobic amino acid residues in conserved positions, here in the positions 305, 308, 309, 312, 313 and 316 of AKAP7δ, form the hydrophobic face of the amphipathic helix and are crucial for RII binding. Small hydrophobic amino acid residues (A, G, V) in the first and last conserved position (305, 316) favour binding [74]. Despite this observation also serine (S305) as it occurs in the wild-type sequence of AKAP7δ mediates binding. If the amino acid residues in the conserved positions are substituted by polar or charged amino acids the affinity is remarkably lowered or abolished. The introduction of proline in the RII-binding domain lowers or abolishes RII binding. The lowered affinity due to the introduction of proline in the positions 300-317 reflects the core binding domain of AKAP7δ, as proline disrupts proper helical folding (see below). Lowered affinity is further observed for certain charged amino acid residues within the core binding domain and flanking regions if substituted by hydrophobic amino acids (e.g. D298, N311). Besides a lowered affinity, introduction of certain

amino acids apparently enhances binding affinity compared to 'wild-type' peptides (distributed throughout the array) as densitometric quantification showed. The most striking enhancement was achieved by the substitutions L304T and L314E. The introduction of an aspartate in positions 305 and 308 (S305D, L308D) abolished binding. Interestingly, S305 is a predicted phosphorylation site for protein kinase C (consensus pattern: [ST]-x-[RK]) and introduction of a negative charge by aspartate mimics phosphorylation in this position. PKA-anchoring by AKAP7-isoforms is therefore putatively regulated by PKC.

Carr and co-workers [93] hypothesised the influence of polar or charged amino acid residues may stabilise the α-helix by forming intra-molecular H-bonds or salt bridges. Enhancement of the apparent binding affinity between peptides and RII subunits by introducing polar or charged amino acid residues (L304T and L314E) raises the question whether the introduced amino acid residues have a direct or an indirect influence on the binding to RII subunits, reflected by differences in the absolute binding affinity and the helical character of the peptides. To answer this questions the binding affinity was determined by surface plasmon resonance (SPR)-measurements and the secondary structure was investigated by circular dichroism (CD)-experiments.

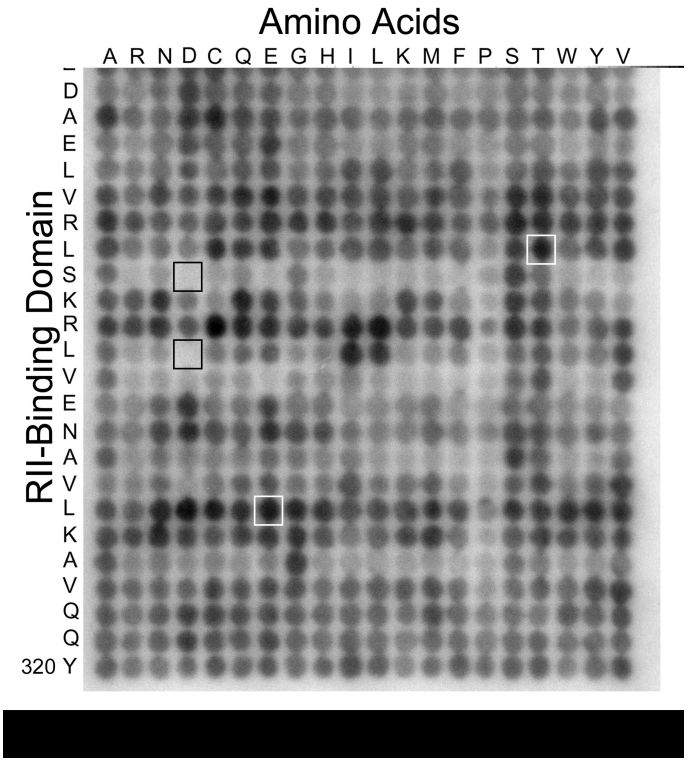

Figure 3.1: Substitution array of the AKAP7δ RII-binding domain. Displayed are peptide-spots from the 25 amino acid residues comprising RII-binding domain of AKAP7δ (Positions 296-320 in AKAP7δ; vertical), that is substituted by any of the 20 biogenous amino acids. Peptides were synthesised on a cellulose membrane and subjected to RII overlay assay. Binding to ^{32}P-labelled RII subunits (bovine RIIα and RIIβ) was detected by autoradiography. Peptides with highest apparent affinity compared to the wild-type sequence are indicated by white boxes. Peptides with completely abolished binding due to the introduced amino acid are boxed in black (amino acids are indicated by their single letter code). The signals were quantified by densitometric analysis. A representative experiment is shown (n=3 independent experiments).

3.2 Determination of the secondary structure and of the RIIα-binding affinity of the AKAP7δ-derived peptides.

Determination of the binding affinity of the AKAP7δ-derived peptides to RII subunits was carried out by SPR-measurements utilising biotinylated peptides as ligands and purified RII subunits as analytes. SPR measurements showed that peptides (25 amino acid residues) representing the RII-binding domain of AKAP7δ (peptide AKAP7δ-wt-pep) bound human RIIα subunits with a K_d value of 0.4 ± 0.3 nM. That was at least one order of magnitude lower than corresponding K_d values obtained using full-length AKAP7δ, truncated AKAP7δ (amino acid residues 124-353) or with the RII-binding peptide Ht31 (see 1.4). Single amino acid substitutions introducing polar or charged amino acid residues (peptides AKAP7δ-L314E-pep and AKAP7δ-L304T-pep) did not significantly change the affinity but the dynamics of the AKAP7δ-derived peptide RII-binding (Fig. 3.2). In the dissociation phase, half maximal binding for the Ht31 peptide is observed at 800 s, whereas for the AKAP7δ-derived peptides (-wt, -L304T and -L314E) only marginal dissociation is observed. By contrast, introduction of two α-helix-disrupting prolines abolished RII-binding (Fig. 3.2, peptides Ht31-P and AKAP7δ-PP-pep). The introduction of a negative charge by replacing leucine with aspartate at position 308 (L308D) also abolished binding to RIIα subunits (Table 3.1).

To investigate whether the introduced polar or charged amino acid residues stabilise the α-helical formation, CD-measurements were carried out utilising the peptides that showed highest apparent or abolished binding to RII

Table 3.1: Binding affinities of AKAP7δ-derived peptides to RII subunits. Displayed are the peptide names, the cognate sequences and the equilibrium dissociation constants (K_d) for the binding to human RIIα (n.b., no binding).

peptide name	**sequence**	**K_d (nM, mean±SEM)**
AKAP7δ-wt-pep	PEDAELVRLSKRLVENAVLKAVQQY	0.4±0.3
AKAP7δ-L314E	PEDAELVRLSKRLVENAVEKAVQQY	0.7±0.5
AKAP7δ-L304T	PEDAELVRTSKRLVENAVLKAVQQY	1.2±1.1
AKAP7δ-L308D	PEDAELVRLSKRDVENAVLKAVQQY	n.b.
AKAP7δ-PP	PEDAELVRLSKRLPENAPLKAVQQY	n.b.

subunits in the peptide substitution array (Fig. 3.1): AKAP7δ-wt, AKAP7δ-L304T, AKAP7δ-L314E and AKAP7δ-L308D, respectively. The CD-spectra display a shoulder at the wavelength of 220 nm typical for an α-helix (Fig. 3.2B). Determination of the α-helical content of the peptides led to similar helicity for the peptides wt-AKAP7δ-pep (72%), L304T-pep (69%), L314E-pep (70%) and L308D-pep (62%). As expected, the α-helical content of the proline containing AKAP7δ-PP-pep was strongly decreased (29%). This indicates that the helical structure is necessary but not sufficient for RII binding peptides as AKAP-derived peptides display similar helicity [84, 74] but differ in binding affinity and the peptide L308D maintains helicity while binding is abolished.

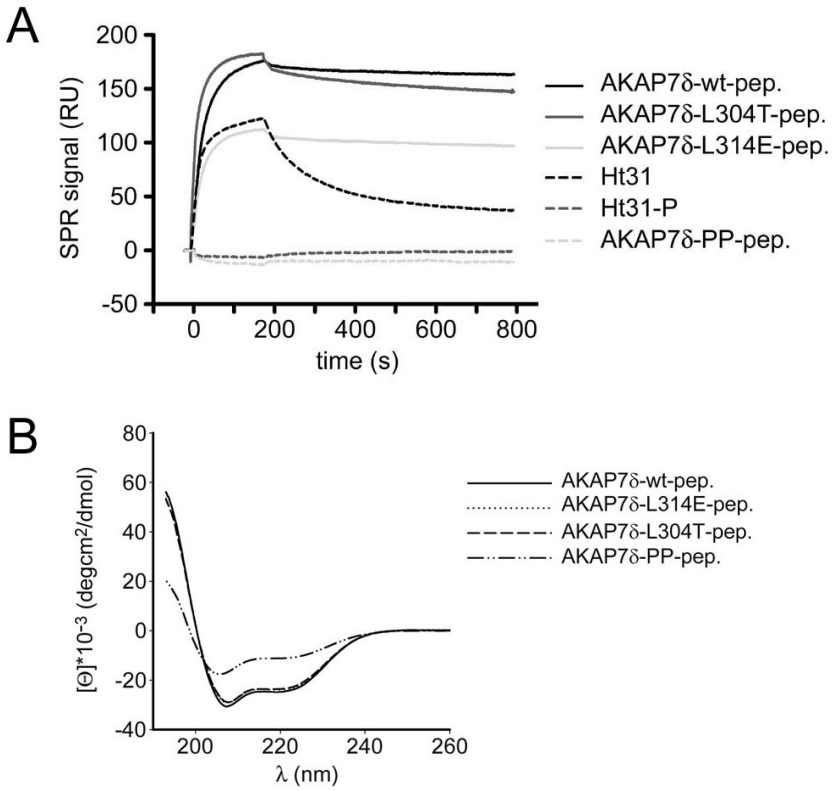

Figure 3.2: AKAP7δ-derived peptides display high affinity RII binding and α-helical secondary structure. A. SPR measurements of the AKAP7δ-derived peptides to determine the association and dissociation rate constants for the binding of the indicated peptides to human RIIα subunits (500 nM). The plots show representative experiments for each interaction (merged plots for comparison of binding dynamics, n=3 independent experiments). RU, resonance units. B. Circular dichroism spectra of the AKAP7δ-derived peptides to determine the α-helicity of the indicated peptides. The helicities (α) of the indicated peptides [each 50 μM in buffer/TFE (1:1, v/v)] were calculated from the mean residue ellipticity [Θ] at 222 nm. Shown are representative spectra from at least three independent measurements of each peptide.

3.3 AKAP7δ-derived peptides inhibit PKA-anchoring in a competitive manner

In order to compare the ability of RIIα subunit binding of AKAP7δ-derived peptides with peptides derived from the RII-binding domains of other AKAPs, a combination of peptide spot technology and RII overlay was utilised. In addition it was tested, whether the AKAP7δ-derived peptides disrupt AKAP-PKA interactions. Peptides (25 amino acid residues) encompassing the RII-binding domains of the human AKAPs, AKAP1, 2, 5, 9, 10, 11, 12, 14, Rab32 and Ht31 peptide, AKAP *in silico* ($AKAP_{IS}$) and AKAP7δ-derived peptides (Fig. 3.3) were spot-synthesised and overlaid with ^{32}P-labelled RIIα subunits. $AKAP_{IS}$ [95] is an RII-binding peptide that has been developed by a bioinformatics approach. Fig. 3.3 shows that AKAP7δ-derived peptides bind RIIα subunits with the highest apparent affinity of all peptides tested. This is supported by the observation that pre-incubation of ^{32}P-labelled RII subunits with peptide AKAP7δ-L314E-pep (10 μM) almost abolished binding to all spot-synthesised peptides, including $AKAP_{IS}$ and Ht31, and strongly decreased its binding to the spot-synthesised peptides AKAP7δ-wt-pep, AKAP7δ-L304T-pep and AKAP7δ-L314E-pep (Fig. 3.3). The control peptide AKAP7δ-PP-pep did not apparently affect the interaction of RIIα subunits with the spot-synthesised peptides, indicating that the AKAP7δ-derived peptide AKAP7δ-L314E-pep is suitable as a potent competitive blocker in RII overlay assays.

The high-affinity binding of AKAP7δ-derived peptides to RIIα subunits suggests that such peptides act as potent disruptors of PKA-anchoring. Human or mouse RIIα subunits (Fig. 3.3) or a combination of bovine RIIα

and RIIβ subunits (Fig. 3.1) bound to spot-synthesised AKAP7δ-derived peptides, Ht31 or AKAP$_{IS}$, indicating that interactions of the peptides with RIIα subunits are not restricted to RII subunits from a particular species.

Peptide-based disruption of PKA-anchoring *in vitro* was further tested on AQP2-bearing vesicles, to which PKA is anchored by AKAP7δ [71, 72]. The peptides AKAP7δ-L314E-pep and Ht31 (each 10 μM) were chosen for the analysis in order to compare their potency to disrupt PKA-anchoring. Each of the peptides decreased PKA activity, HT31 by 29-53% and AKAP7δ-L314E-pep by 31-63% compared to PKA activity of untreated AQP2-bearing vesicles (Fig. 3.4). The control peptide AKAP7δ-L308D-pep, which does not bind RII subunits (Table 3.1) did not affect PKA activity. The PKA inhibitor peptide PKI-(5-24) ablated vesicular PKA activity (see Discussion).

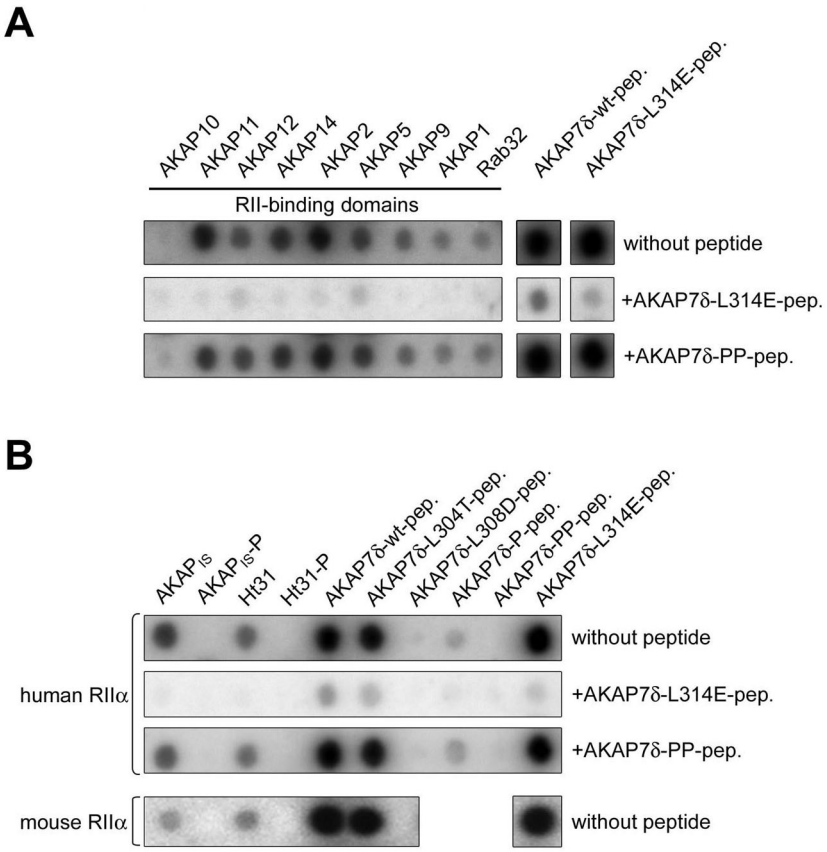

Figure 3.3: AKAP7δ-derived peptides act as PKA-anchoring disruptors *in vitro*. A. Peptides derived from the RII-binding domains of the indicated AKAPs, and peptide AKAP7δ-L314E-pep were spot-synthesised and probed with human ^{32}P-labelled RIIα subunits alone, in the presence of the PKA-anchoring disruptor peptide AKAP7δ-L314E-pep (10 μM) or the inactive control peptide AKAP7δ-PP-pep (10 μM) as indicated. B. Peptides representing the RII-binding domain of AKAP7δ, derivatives thereof, Ht31 and AKAP$_{IS}$ were spot-synthesised and probed with human or mouse ^{32}P-labelled RIIα subunits alone, in the presence of the PKA-anchoring disruptor peptide AKAP7δ-L314E-pep (10 μM) or the inactive control peptide AKAP7δ-PP-pep (10 μM) as indicated. Signals were detected by autoradiography. Representative experiments are shown (n=3 independent experiments).

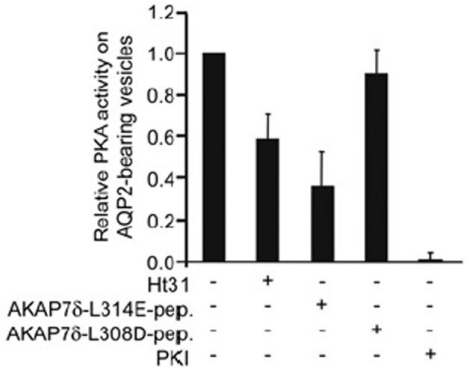

Figure 3.4: AKAP7δ-derived peptides displace PKA activity from AQP2-bearing vesicles. AQP2-bearing vesicles were isolated from rat renal inner medullary tissue. The vesicles were left untreated or incubated with the peptides Ht31, AKAP7δ-L314E-pep, AKAP7δ-L308D-pep (100 μM each) or the PKA inhibitor peptide PKI (100 μM) and PKA activity was assayed (n=3; means $\pm$ SEM).

3.4 AKAP7δ-derived peptides function as AKAP-PKA disruptors *in vivo*

The efficiency of the AKAP7δ-derived peptides to disrupt PKA-anchoring in a cellular system was evaluated by interference with PKA-anchoring in neonatal cardiac myocytes and inner medullary collecting duct (IMCD) cells derived from rat kidneys. In cardiac myocytes, L-type Ca^{2+} channels are phosphorylated by PKA in response to β-adrenergic receptor activation [88, 89, 90]. Phosphorylation increases the open-probability of the channels and is a key event in β-adrenergic-receptor-mediated increases in myocyte contractility. Global uncoupling of PKA from AKAPs with the peptide Ht31 prevented β-adrenergic receptor-mediated increases in L-type Ca^{2+} channel currents in adult rat cardiac myocytes [88, 89]. Additionally, an AKAP7α-derived peptide mimicking the domain (leucine-zipper motif) of AKAP7α that mediates direct interaction with L-type Ca^{2+} channels had a similar effect [89]. Fig. 3.5 depicts patch-clamp experiments using rat neonatal cardiac myocytes which show that the peptides AKAP7δ-L304T-pep and AKAP7δ-L314E-pep also prevented isoproterenol (β-adrenergic receptor agonist)-induced PKA-dependent increases in L-type Ca^{2+} channel currents in these cells at a concentration of 30 μM. Peptide AKAP7δ-wt-pep was partially insoluble at a concentration of 30 μM and was therefore used at 1 μM. At this concentration it prevented the isoproterenol-induced increase in L-type Ca^{2+} channel current to the same extent as the peptides AKAP7δ-L304T-pep and AKAP7δ-L314E-pep. The control peptide AKAP7δ-PP-pep, which does not bind RIIα subunits, did not alter L-type Ca^{2+} channel currents at either 1 or 30 μM concentration (Fig. 3.5).

Stearate-coupled or myristoylated versions of the peptide Ht31 disrupt PKA-anchoring in IMCD cells [98]. AKAP7δ-derived peptides AKAP7δ-L314E-pep and AKAP7δ-PP-pep were coupled to stearate (S-AKAP7δ-L314E-pep and S-AKAP7δ-PP-pep, respectively) and tested for their cellular effects by visualising the subcellular distribution of AQP2 in IMCD cells (Fig. 3.6). Under resting conditions, AQP2 is localised mainly on intracellular vesicles [72]. Upon enhancing the level of intracellular cAMP (either by AVP stimulation of the V2R or by direct stimulation of the ACs with forskolin) AQP2 channels redistribute to the plasma membrane. Incubation with anchoring disrupting peptides prevents AQP2 redistribution upon stimulation [98, 71, 72]. Thus, the redistribution depends on PKA activity and anchoring. Treatment with the stearate-coupled (S-) anchoring disrupting peptide AKAP7δ-L314E (Fig. 3.6 D) prevented AVP-induced AQP2 redistribution to the plasma membrane compared to the negative control peptide AKAP7δ-PP (Fig. 3.6 F) or IMCD cells without peptide treatment (Fig. 3.6 B). Peptide treatment without AVP stimulation of the IMCD cells (Fig. 3.6 C, E) did not change subcellular distribution of AQP2 compared to untreated cells (Fig. 3.6 A). Taken together, the results show that the AKAP7δ-derived peptides act as potent PKA-anchoring disruptors *in vitro* and *in vivo*.

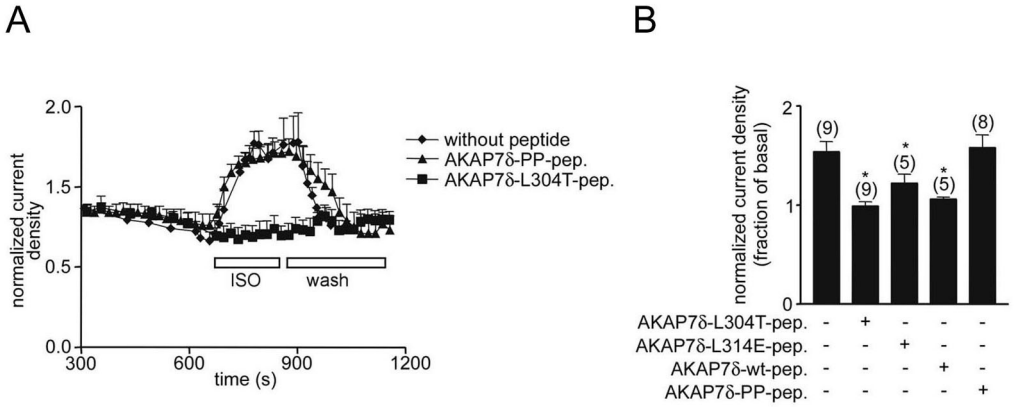

Figure 3.5: AKAP7δ-derived peptides act as PKA-anchoring disruptors *in vivo* abolishing β-adrenoceptor induced L-type Ca-channel currents. L-type Ca^{2+}-channel currents were measured in rat neonatal cardiac myocytes by using the patch-clamp technique. Cells were clamped to -70 mV and repetitively depolarised to a test potential of 0 mV after a 400 ms ramp to -35 mV. The peptides AKAP7δ-L304T-pep, AKAP7δ-L314E-pep or the inactive control peptide AKAP7δ-PP-pep (30 μM each) and AKAP7δ-wt-pep (1 μM) were administered through the patch pipette. Current recordings started 400 s after establishing whole-cell configuration. Cells were stimulated with isoproterenol (1 μM; ISO) at the indicated time followed by a washout. Time courses of normalised current densities (A) and a summary (B) of the individual experiments (n is indicated by the numbers in brackets, means $\pm$ SEM). *, significant difference from untreated control ($P<0.05$).

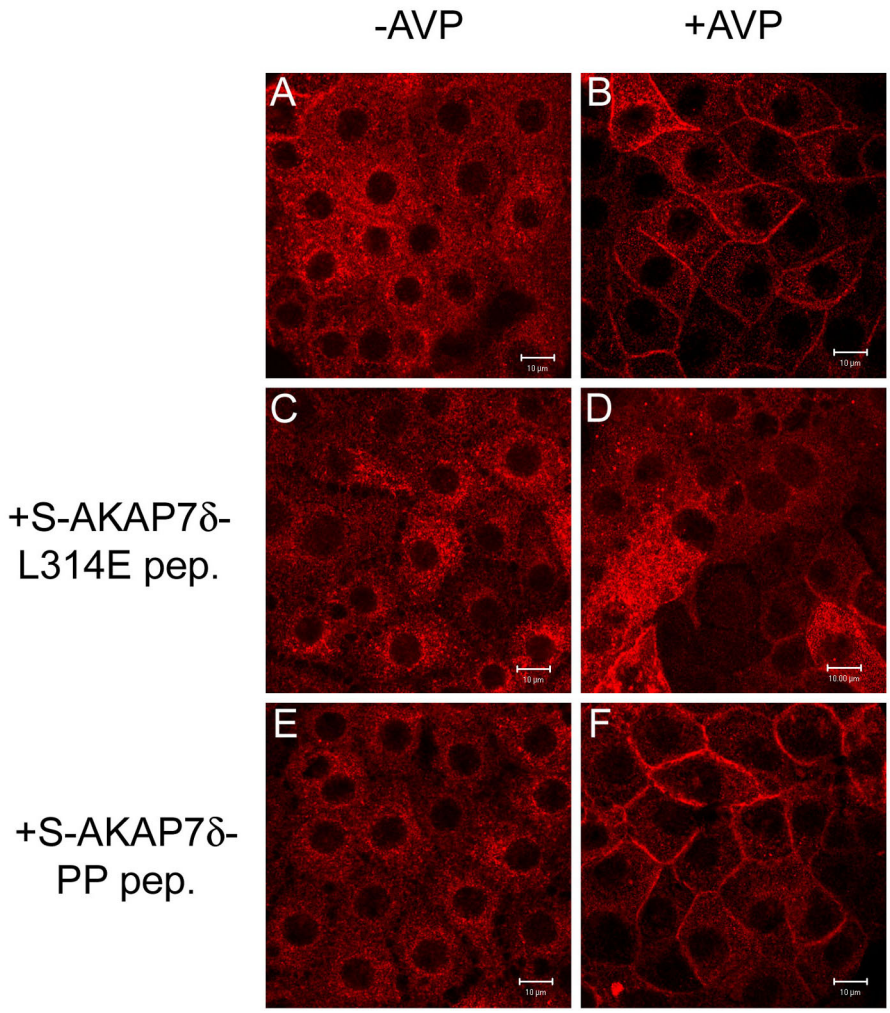

Figure 3.6: AKAP7δ-L314E peptide acts as PKA-anchoring disruptor *in vivo* preventing redistribution of AQP2 from cytosol to the plasma membrane in IMCD-cells. IMCD cells were pre-incubated with the stearate-coupled (S-) AKAP7δ-L314E (C, D), the negative control peptide AKAP7δ-PP (E, F; 100μM for 30 min each) or left untreated (A, B), followed by stimulation with AVP (100 nM, 15 min ; B, D, F) or left untreated (-AVP; A, C, E) . Thereafter cells were fixed, permeabilised, and immuno-stained with a specific anti-AQP2 antiserum (rabbit) and Cy3-coupled secondary antibody (goat, anti-rabbit antibodies) and analysed by confocal laser scanning microscopy (bar indicates 10 μM).

3.5 Determinants of high affinity PKA-anchoring

Next the molecular basis of the high affinity interaction between the RII-binding domain of AKAP7δ and RII subunits was investigated. An alignment of the RII-binding domains of 18 known AKAPs (Fig. 3.7) indicated the presence of mainly hydrophobic (shaded in grey) amino acid residues in conserved positions as published previously [73, 95]. A peptide substitution array of the AKAP7δ RII-binding domain (Fig. 3.1) also documented the relevance of hydrophobic amino acid residues in conserved positions and, in addition, the efficiency of proline to lower or disrupt RII-binding (see Fig. 3.1, Fig. 3.2, Fig. 3.3 and Table 3.1). Molecular modelling of the interaction between the RII-binding domain of AKAP7δ (amino acid residues 296-320) and RIIα subunits (amino acid residues 1-44; Fig. 3.8) again revealed hydrophobic contacts. The amino acid residues involved correspond to those suggested by the alignment depicted in Fig. 3.7. In addition, the model suggested that polar and charged amino acid residues within the RII-binding domain contribute to the interaction. Seven out of 13 such amino acid residues may form hydrogen bonds (E297, E300, S305, K306, N311, K315 and Q319) with partners of the RIIα dimer (protomers are distinguished by apostrophes). One amino acid residue (D298) may form a salt bridge with R′24 of RIIα and one (K306) may form either a hydrogen bond with Q′16 or a salt bridge with E′13 of RIIα. This is depicted schematically in Fig. 3.8 B, which also indicates potential hydrogen bonds and salt bridges between the peptides AKAP7δ, AKAP7δ-L314E-pep, Ht31 and AKAP$_{IS}$ and RIIα subunits.

In order to test whether non-hydrophobic contacts play a role in the in-

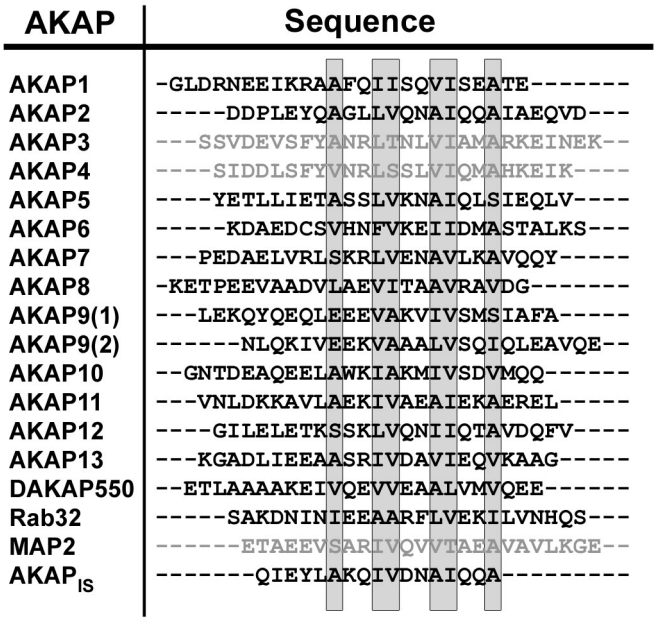

Figure 3.7: Multiple sequence alignment of RII-binding domains of the indicated AKAPs. Amino acid residues in conserved positions are shaded in grey. The two RII-binding domains of AKAP9 are indicated by (1) and (2). RII-binding domains containing polar amino acids residues in the central conserved positions are depicted in grey.

teraction between AKAP7δ and RIIα subunits, a peptide encompassing the RII-binding domain of AKAP7δ (amino acid residues 295-323), and a series of truncation mutants of this peptide, were spot-synthesised and probed with ^{32}P-labelled RIIα subunits (Fig. 3.9). N-terminal truncations of 1-5 amino acids removed three predicted interacting residues (E297, D298 and E300) from the RII-binding domain. C-terminal truncations of 1-6 amino acids removed one residue (Q319) predicted to be involved in the interaction. Indeed, removing the relevant amino acid residues at either the N- or C-terminus resulted in decreased RII-binding (Fig. 3.9). Next, the influences of single amino acid residues in the RII-binding domain of AKAP7δ that potentially form hydrogen bonds or salt bridges with residues of RIIα subunits were

tested by utilising a combination of peptide spot-synthesis and RII overlay. For this purpose, the peptide AKAP7δ-wt-pep and versions thereof with alanine substitutions at the relevant positions (Fig. 3.10) were spot-synthesised and probed with ^{32}P-labelled RIIα subunits. Fig. 3.10 A shows that the replacement of the charged amino acid residues D298 and E300 by alanine decreased binding to a similar extent as a N-terminal truncation, removing these residues from peptide 5 as shown in the Fig. 3.9 (upper panel). Similarly, both substitution of the polar Q319 with alanine or its removal by truncation as in peptide 6, shown in Fig. 3.9 (lower panel), decreased the binding to RII subunits. The substitution of alanine in position 311 for asparagine (N311A) led to a strong decrease in RIIα subunit binding (Fig. 3.10 A). This asparagine is conserved in the high-affinity AKAPs, AKAP7δ, AKAP2, AKAP5, AKAP12, and in AKAP$_{IS}$ (Fig. 3.7). The substitutions of alanine in positions 306 and 315 for lysine (K306A, K315A) also led to a strong decrease in RIIα subunit binding, for lysine in position 306 positive charged amino acid residues are conserved in the AKAPs, AKAP7δ, AKAP3, AKAP6, AKAP9(1), AKAP11, Rab32 and in AKAP$_{IS}$. The peptides AKAP7δ-wt-pep, AKAP7δ-L314E-pep, and derivatives of the latter in which all potential hydrogen-bond- or salt bridge-forming amino acid residues were replaced by alanine in all possible combinations (512 peptides, Fig. 3.10 B). These peptides display a general decrease in RIIα subunit binding with raising numbers of substitutions. Within a set of such peptides containing the same number of substitutions, peptides with distinct combinations of substitutions show a stronger reduction in RIIα binding consistent with the strong decrease in RIIα binding for distinct single amino acid substitutions as described above. None of the tested alanine-substituted peptides lost the

ability to bind to RIIα subunits (Fig. 3.10), suggesting that the interaction mediated by hydrophobic amino acid residues is retained in the peptides. Taken together, the results indicate that hydrophobic amino acid residues in the amphipathic helix form the backbone for the interaction of the AKAP7δ RII-binding domain with RII subunits and, in addition, that the binding is increased by charged and polar amino acid residues on the hydrophilic face of the helix, presumably through intermolecular hydrogen bond or salt bridge formation.

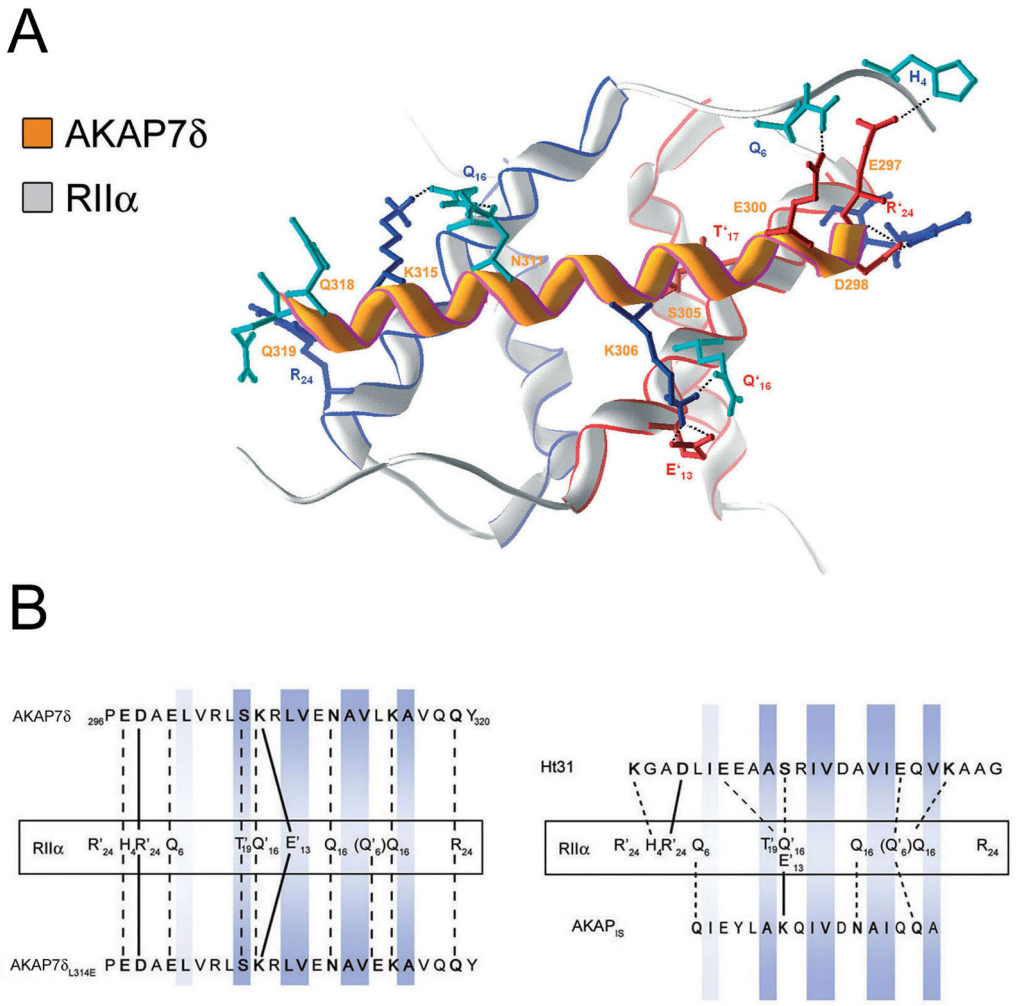

Figure 3.8: Model of the interaction between the RIIα dimer and AKAP-derived peptides. A. Structural model showing the interaction (top view) of the RII-binding domain of AKAP7δ (helix, orange, residues 296-320 of AKAP7δ) with the dimer of RIIα subunits (the light grey backbones of the two monomers are verged in red and blue respectively). Essential interacting hydrophilic side-chains of polar (cyan) or charged (red, negative; blue, positive) amino acid residues are displayed and labelled (single letter code and position within the protein). B. Schematic representation of the interaction between RIIα subunits and the RII-binding domain of AKAP7δ (corresponds to peptide AKAP7δ-wt-pep) and the peptides AKAP7δ-L314E-pep (left panel), Ht31 and AKAP$_{IS}$ (right panel). Amino acid residues that potentially form hydrogen bonds or salt bridges are connected by dotted and unbroken lines, respectively. Hydrophobic amino acid residues in conserved positions are shaded in blue. The residues of the two RIIα protomers are distinguishable by the absence and presence of apostrophes.

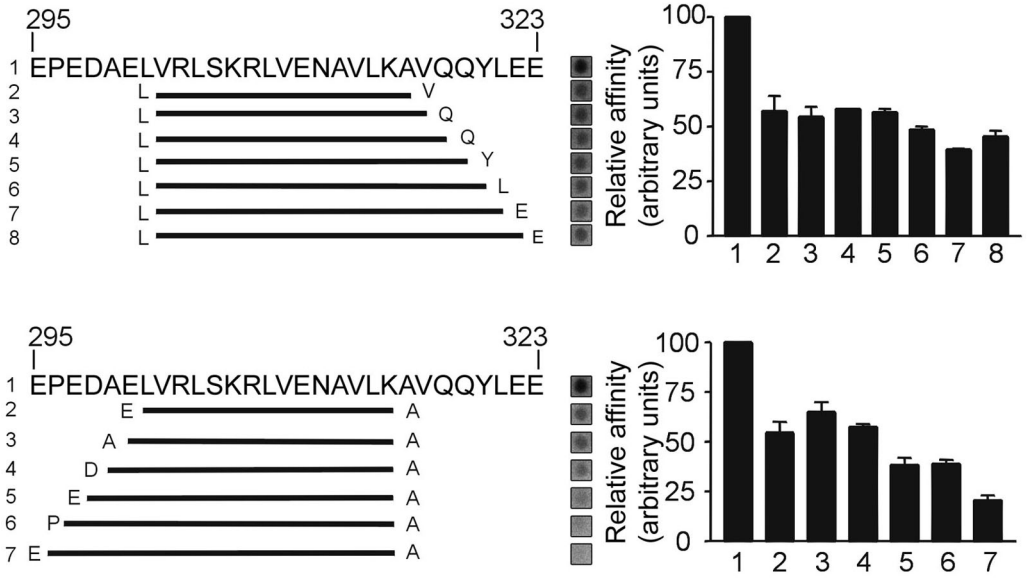

Figure 3.9: Influence of amino acids flanking the core RII-binding domain of AKAP7δ. The peptides comprising the extended RII-binding domain of AKAP7δ (amino acids 295-323 of AKAP7δ) and the indicated N- and C-terminally truncated versions (black lines) were spot-synthesised and probed with ^{32}P-labelled RIIα subunits. Interaction was detected by autoradiography. Representative spots from three independent experiments are shown. The signals were quantified by densitometric analysis, relative affinity of each peptide for RIIα binding is depicted as the ratio of its signal intensity to that of the peptide AKAP7δ-wt-pep (mean $\pm$ S.D.). The numbers in the left and right panels denote the same peptides.

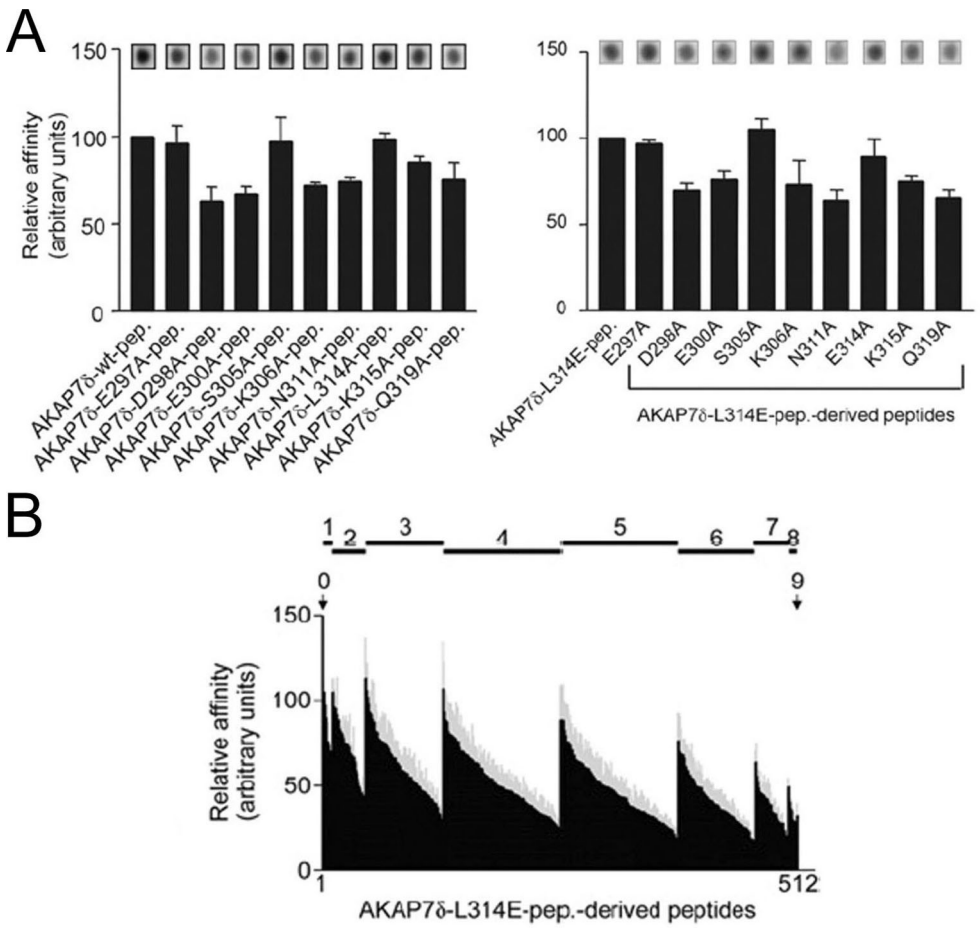

Figure 3.10: Contribution of amino acid residues in non-conserved positions to the AKAP-RII binding. A. Peptide substitution arrays were generated and subjected to RII overlay where each potential hydrogen bond- or salt bridge-forming amino acid residue of the peptides AKAP7δ-wt-pep (left panel) and AKAP7δ-L314E-pep (right panel) was substituted with alanine. The peptides were probed for binding to ^{32}P-labelled RII subunits. Representative data from three independent experiments are shown. Signals were visualised by autoradiography and quantified densitometrically. Relative binding affinities of each peptide, normalised to that of the peptide AKAP7δ-wt-pep (left panel) or AKAP7δ-L314E-pep (right panel, means ± SEM). B. The peptides AKAP7δ-wt-pep, AKAP7δ-L314E-pep, and derivatives of the latter in which all potential hydrogen-bond- or salt bridge-forming amino acid residues were replaced by alanine in all possible combinations (512 peptides) were spot-synthesised. The peptides were subjected to RII overlay assays and analysed as described in A (means ± SEM, grey). Indicated are: numbers of amino acid residue substitutions (top of the graph) and sets of peptides containing the same number but different combinations of substitutions (black lines). Within each set the peptides are ordered according to their relative affinity.

3.6 A bioinformatics-based approach to identify new AKAPs

Hydrophobic amino acid residues in conserved positions serve as important contacts for AKAP-PKA binding, which has been demonstrated previously and in this work [73, 76]. A consensus pattern was provided by Vijayaraghavan *et al.* [76] that summarised these properties, suitable for determining RII-binding domains within a given AKAP. Searching a protein database for AKAPs turned out to be impossible with this very general pattern as it provided too many hits. The model of H-bonds and salt bridges that directly influence AKAP-RII-binding provided the possibility to restrict such a database search, and furthermore does the peptide-spot technique provide an excellent method to test candidates derived from a database in a high throughput approach.

Assuming that the number and positions of amino acids that function as acceptors or donors of H-bonds or salt bridges vary amongst AKAPs, a description of such amino acids in a pattern is not suitable. On the other hand charged amino acid residues (putative salt bridge or H-bond partners) influence the calculated isoelectrical point (P_I) of a peptide, independently of their position. If the charged amino acid residues influence the RII-binding the calculated P_I for RII-binding domains should be limited to a certain range. The P_I in turn can be utilised to restrict a database search. The calculated P_I for the peptides represented (Fig. 3.7) the range from 3.39 - 6.19 (for AKAP2 and AKAP3, respectively). Thus, restricting the theoretically possible range for 25-mer peptides of 2.6 - 13.0 (for peptides consisting exclusively of glutamate or arginine, respectively) to less

than a third. Taking into account that the dimerisation and docking domain of the RII dimer forms a symmetric groove (Fig. 3.8 [83]), two fold mirror symmetry for the RII-binding domains was assumed for a pattern derived from the amino acid residues in conserved positions (displayed in Fig. 3.7; conserved positions are shaded in grey; sequences depicted in grey were neglected, see Discussion): [AVLISE]-X-X-[AVLIF][AVLI]-X-X-[AVLI][AVLIF]-X-X-[AVLISE], amino acids in square brackets denote alternatives whereas X stands for any amino acid. Utilising this pattern and limiting the P_I-range to 3.0 - 6.4 the swissprot database was searched for protein data subsets of several model organisms (*Dictyostelium discoideum, Saccharomyces cerevisiae, Drosophila melanogaster, Danio rerio, Mus musculus, Rattus norvegicus, Homo sapiens*) with the scansite program (http://scansite.mit.edu/) . The search retrieved approximately 11700 hits. To reduce this number only the subset of human proteins was further investigated. The cognate sequences of each ID-entries were retrieved utilising the bioperl package. Amino acid sequences following the pattern extended for 9 or 4 amino acid residues at the C- or N-terminus of the hit sequence to obtain 25-mers were extracted resulting in 4519 peptides derived from 2352 proteins. These peptides were further filtered in order to exclude duplicates and undesired peptides, compare 2.3) resulting in 2572 peptides that were spot-synthesised and subjected to RII overlay assay. The excluded undesired peptides divide into 10.5% 'difficult sequences', 0.1% proline containing, 14.9% putative turn-building and 74.5% cysteine containing sequences. Thus the RII-binding domain of AKAP6 was excluded as it contains a cysteine residue (see 3.7). This bioinformatics-based approach to identify new AKAPs is summarised in Fig. 3.11.

Of the 2572 peptides approximately a third (829) displayed a signal in the autoradiograph. These peptides were probed again for RII binding (Fig. 3.12). To exclude false positives (peptides that bind to RII subunits in a non-AKAP manner) all positive peptides were spot-synthesised again and probed in a competitive RII overlay with human ^{32}P-RIIα subunits pre-incubated with AKAP7δ-L314E-peptides, with the negative control peptide AKAP7δ-PP or left untreated. Of the 829 peptides 27 peptides (and additionally 9 derived from previously described AKAPs) displayed reduced or abolished binding in the competitive RII overlay assay. Of the remaining peptides that did not show apparent reduced binding one derived from RHG4 (Rho GTPase-activating protein 4, also named p115) was utilised as a (non-AKAP) positive control and peptides were probed again for competitive RII-binding (Fig. 3.13). Peptides that showed reduced or abolished signals in the presence of AKAP7δ-L314E-peptides derived from previously identified AKAPs or were treated as candidates representing new RII-binding domains (Fig. 3.13). Prediction of the secondary structure (Psipred) of these candidate peptides revealed high probability to form α-helices for all candidates. Amongst proteins containing candidate RII-binding domains one, CN129, was chosen to be tested whether the cognate protein functions as AKAP, as its protein structure was solved previously (see 3.10). The sequence of the putative RII-binding domain of the protein CN129 is TDMKDMRLEAEAVVNDVL-FAVNNMF. CN129 is named after its chromosomal localisation, chromosome 14, open reading frame 129 (swissprot-ID: CN129_ HUMAN) is highlighted in Fig. 3.11B, 3.12 and 3.13 (black box).

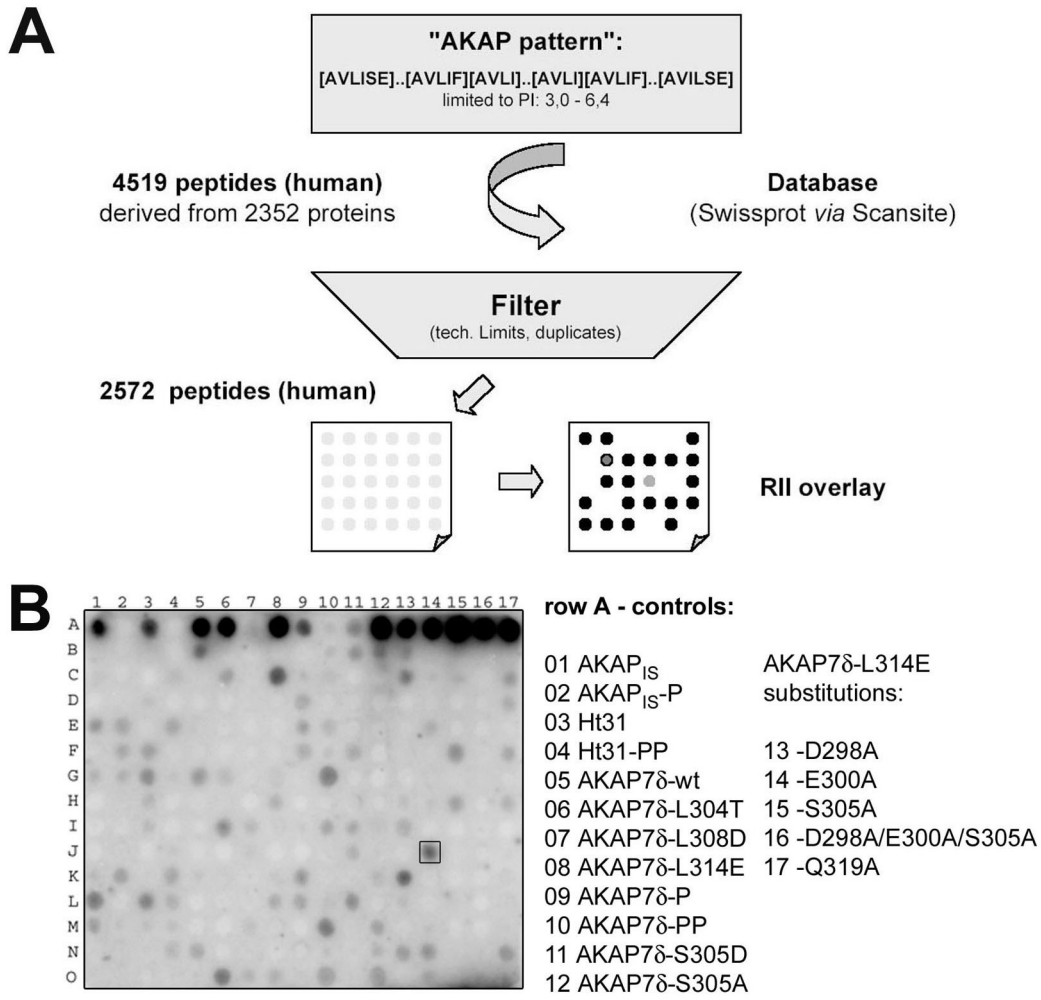

Figure 3.11: A bioinformatics approach to identify new AKAPs. A. Flow chart for the identification of RII-binding domains from a protein database. Schematically depicted are the AKAP pattern (regular expression) for the swissprot database search, the limitation to a P_I of 3.0 - 6.4, a filter step to reduce duplicates and undesired peptides, the spot synthesis and detection by RII overlay assay. The amount of peptides obtained from each step prior to detection of RII-binding is indicated. B. Approximately a third of all peptides bind RIIα. Shown is the autoradiography of one membrane comprising 255 peptides. Row A contains control peptides. Altogether the 2572 peptides were synthesised on 11 membranes and assayed for RII-binding by RII overlay assay. Amongst the peptides binding to RII subunits, one derived from the protein CN129 was chosen for further investigation (J14, black box).

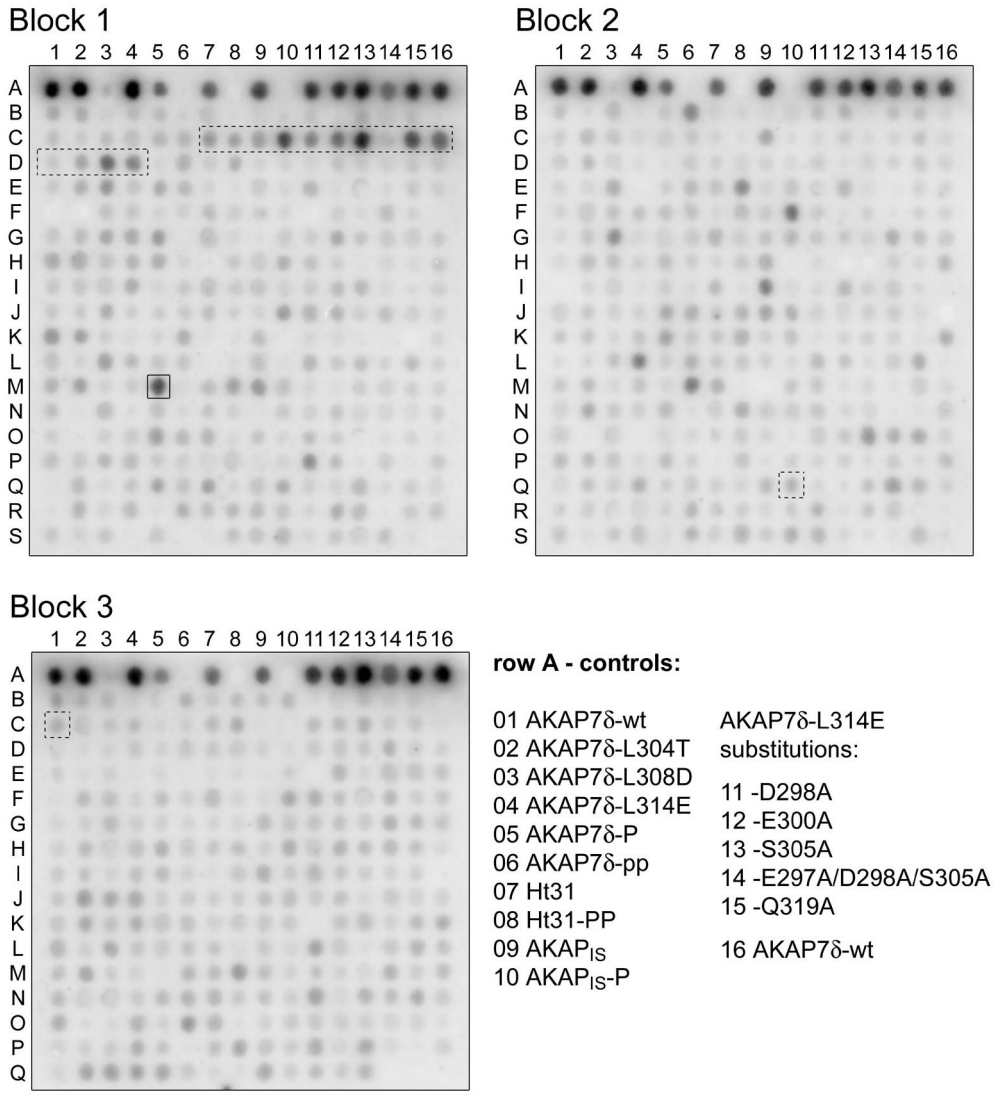

Figure 3.12: All 829 of the 2572 peptides that bound RIIα in the RII overlay assay. Displayed are the 829 spot-synthesised peptides tested again for RIIα binding. These peptides from the database search bound RIIα in the initial RII overlay assay and were distributed over 11 membranes. Row A of each block represents control peptides as indicated. The AKAP7δ-derived peptides show highest apparent affinity amongst all peptides tested (autoradiography). Peptides derived from previously identified AKAPs (dotted boxes) and from CN129 (solid box) are indicated. Peptides are sorted according to their swissprot identifiers, for a complete list of all tested peptides see Appendix B.

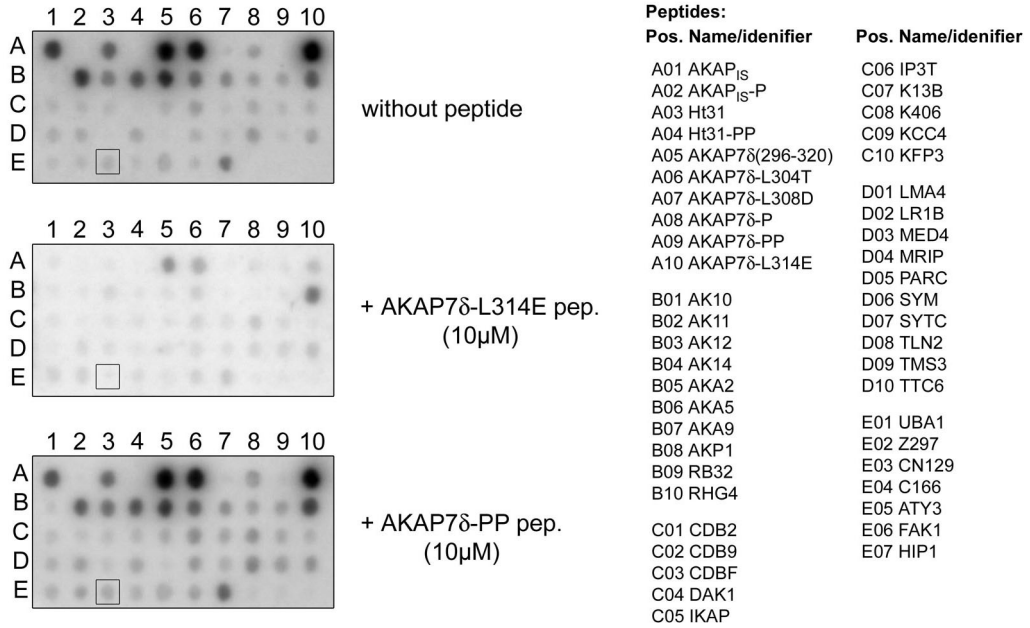

Figure 3.13: Peptide assay for competitive RII-binding. Of the 829 peptides that bound RIIα 27, not described as AKAPs, showed a reduced or no signal in the presence of AKAP7δ-L314E-pep but RIIα-binding in the presence of the negative control peptide AKAP7δ-PP-pep. Displayed are these peptides, tested again for competitive RIIα-binding. Row A of each block represents control peptides as indicated, row B represents peptides derived from previously identified AKAPs and a peptide derived from the RHG4 protein (B10) that did not show reduced apparent binding affinity upon peptide treatment.

3.7 The CN129 protein functions as AKAP *in vitro*

The CN129 protein was identified as putative new AKAP. To characterise the cognate RII-binding domain an array of overlapping peptides and a peptide substitution array of the putative RII-binding domain were probed for RII-binding. The array of overlapping peptides (25-mers, shift 1) covering the complete CN129 protein (139 amino acids, calculated molecular weight: 15,6 kDa) was spot-synthesised and subjected to RII overlay assay. The cysteines in positions 5, 59 and 77 within the CN129 peptide sequence were substituted by serine (see 3.1). The autoradiography revealed that the previously identified peptide (TDMKDMRLEAEAVVNDVLFAVNNMF) is indeed the peptide with the highest apparent binding to RII subunits within the CN129 sequence (Fig. 3.14). The overlapping peptides show a pattern of RII binding expected for a linear organised domain with decreasing affinity upon increasing distance from the region of maximal binding. However, additional peptides with weak apparent binding were detected (see Discussion).

The autoradiography of the peptide substitution array of CN129 displayed a clearly reduced or abolished apparent binding if hydrophobic amino acid residues in conserved positions are substituted by polar or charged amino acid residues (Fig. 3.15, solid boxes). The reduction of apparent binding by proline reflects the helical core binding domain of CN129 (dotted box, compare Fig. 3.1 and Fig. 3.19) indicating typical AKAP properties.

To investigate whether the CN129 protein functions as an AKAP, fusion proteins of CN129 and cyan fluorescent protein (CFP) were generated. Therefore, the human cDNA of CN129 derived from human

neuroblastoma cells (SH-SY5Y) and the rat orthologue cDNA derived from rat brain were cloned into a CFP-vector (pECFP-N1). A mutant that contains two prolines in the putative RII-binding domain (TDMKDMRLEAEAVPNDVPFAVNNMF, see Fig. 3.15) was generated as a negative control. The CN129-CFP-fusion proteins were overexpressed in HEK293 cells, precipitated from cell lysates and tested for AKAP function in two ways. First, the immune-precipitated (anti GFP-antibody, rabbit) fusion proteins were separated by SDS-Page and blotted to PVDF-membranes. Membranes were subjected to a competitive RII overlay assay. Untreated immune-precipitates displayed a double band at the expected molecular weight in the autoradiography not observed in the pre-immune controls. Upon treatment with the RII-binding inhibitor AKAP7δ-L314E (10 μM) RII binding to CN129-CFP fusion proteins and AKAP7δ-YFP were abolished. Second, the partial human CN129-CFP fusion proteins (amino acids 1 - 125) comprising the double proline mutation were immune-precipitated and subjected to RII overlay for detection of RII-binding as described. The human partial CN129-CFP-fusion protein displayed a signal in the autoradiography at the appropriate molecular weight whereas the proline-mutant did not. An additional prominent protein band is detected at approximately 66 kDa in immune-precipitates and in pre-immune controls. Its identity is unknown. These experiments clearly provide evidence for the AKAP function of the CN129 protein *in vitro*.

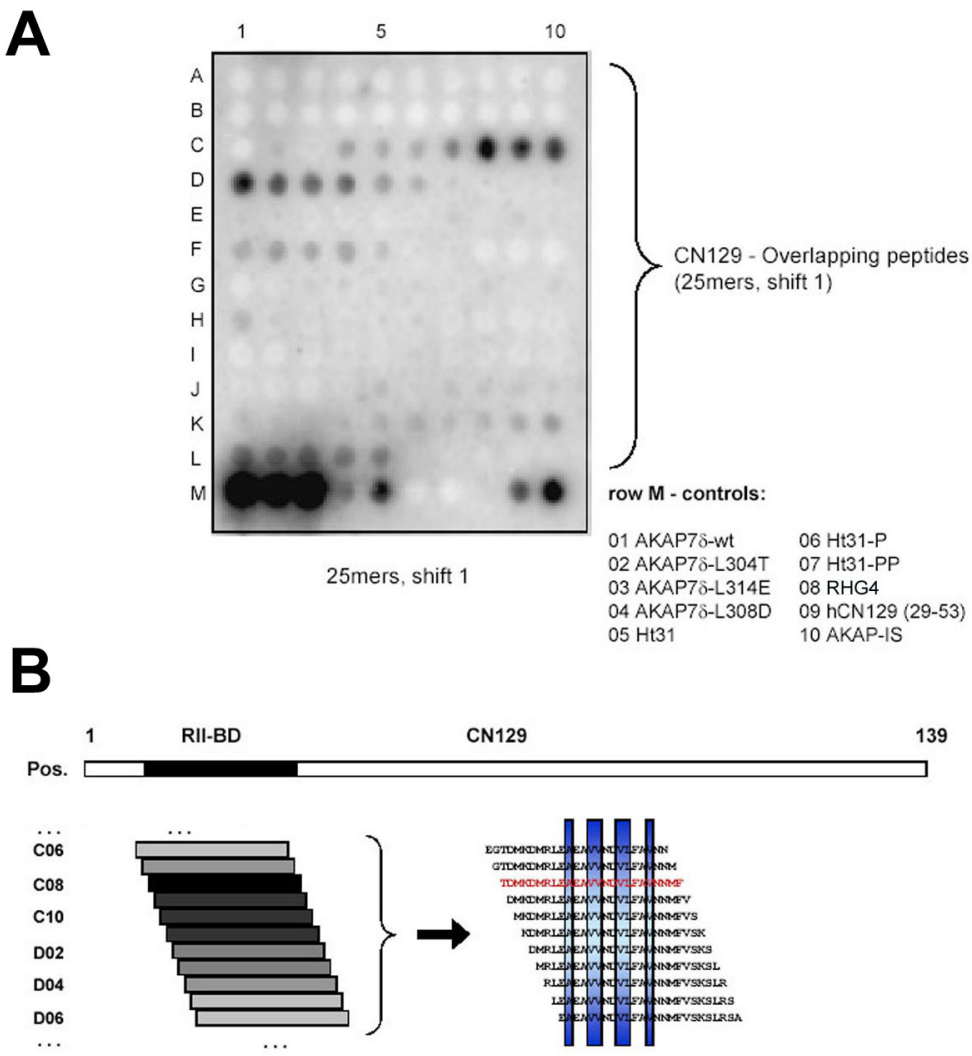

Figure 3.14: Mapping the RII-binding domain of CN129. The peptide sequence of CN129 (139 amino acids) was spot-synthesised as overlapping peptides (25-mers) with a shift of one amino acid. A. Autoradiography of the overlapping peptides assayed by RII overlay. The control peptides are indicated (row M). B. Scheme of the overlapping peptides derived from CN129. The previous identified RII-binding domain (black bar) and the flanking region (grey bars) corresponding to the spots in B are indicated and sequences are displayed (conserved positions are shaded in blue).

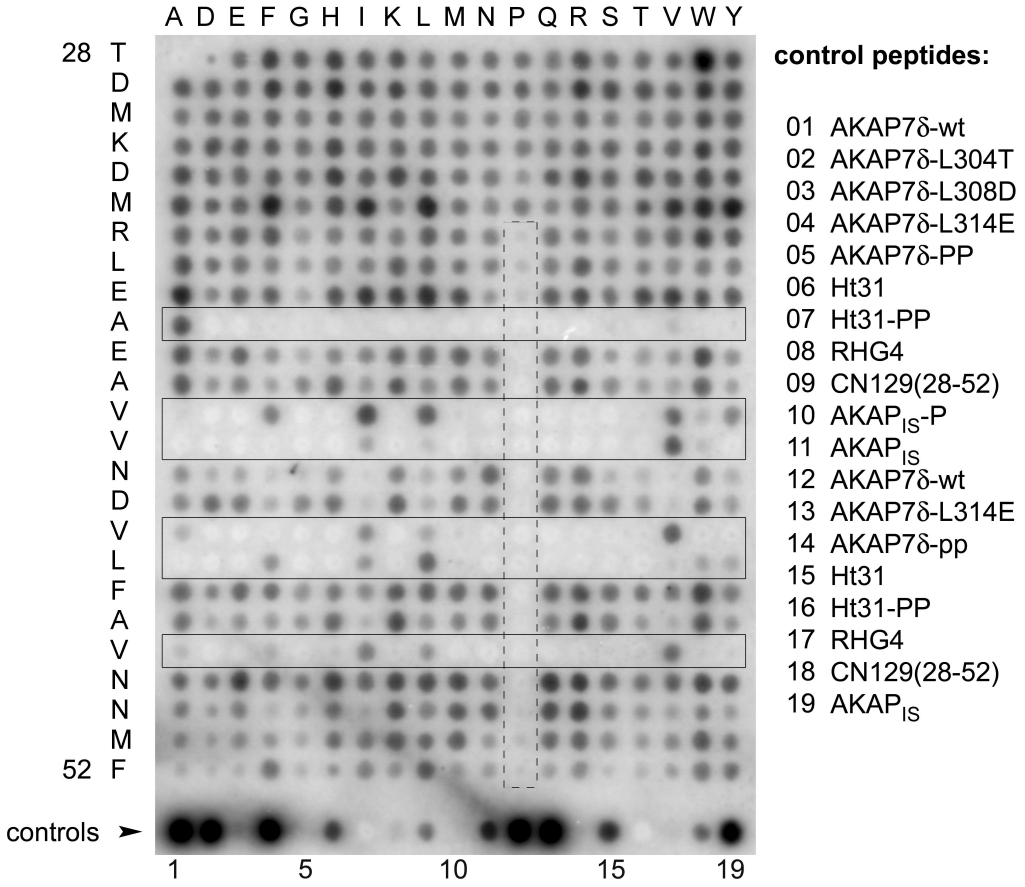

Figure 3.15: Substitution array of the CN129 RII-binding domain. Displayed are peptide spots from the putative RII-binding domain of CN129 (Positions 28-52; vertical), that is substituted by the biogenous amino acids (horizontal). Spot-synthesised peptides were subjected to a RII overlay assay. Binding to human ^{32}P-labelled RIIα subunits was detected by autoradiography. The substitutions for amino acid residues in conserved positions are indicated (solid black boxes). Substitution by proline in the core binding domain reduces or abolishes binding (doted black box; amino acids are indicated by their single letter code, control peptides as indicated).

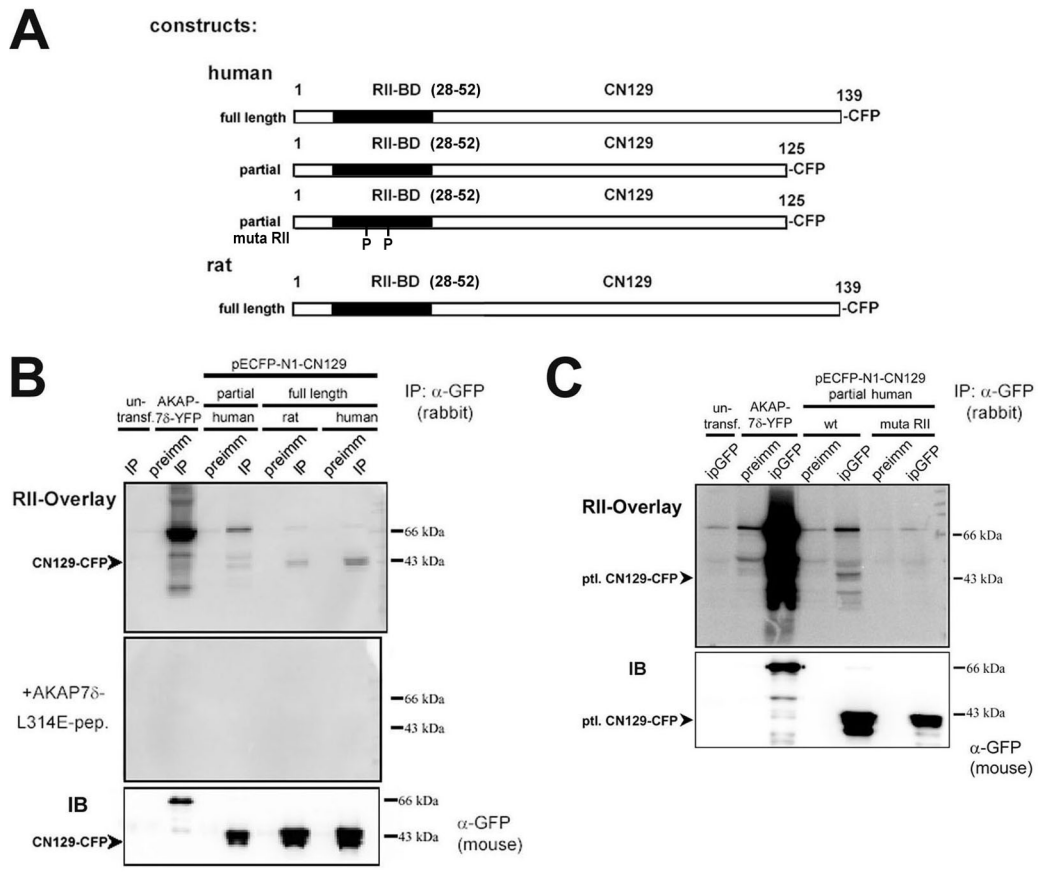

Figure 3.16: CN129 functions as AKAP *in vitro*. A. Scheme of the CN129-CFP fusion constructs. The length of the constructs, the positions of the RII-binding domain, the proline point mutations and the CFP-tag are indicated. B. CFP-fusion proteins of CN129 (rat, human partial and full length and AKAP7δ-YFP as control were overexpressed in HEK293 cells. Cell lysates from untransfected and transfected cells were incubated with anti-GFP antibody (α-GFP, rabbit) or pre-immune serum. The thus yielded immunoprecipitates were separated by SDS-Page and blotted to PVDF-membranes. Membranes were subjected to RII overlay assay and detected by autoradiography. RII overlay was performed without (upper panel) or with the anchoring disruptor AKAP7δ-L314E-pep (10 μM, middle panel, 45% of samples, each). An immunoblot (IB) was performed as loading control (lower panel, residual 10% of samples) utilising anti-GFP (α-GFP, mouse) as primary and peroxidase-coupled anti-mouse as secondary antibody. C. The CFP-fusion protein of CN129 (human, partial), a double proline mutation (muta RII, see text) of this construct and AKAP7δ-YFP as control were overexpressed in HEK293 cells and treated as described above. An immunoblot was performed as loading control (lower panel, 10% of samples). Molecular weights of the marker are indicated.

3.8 Subcellular distribution of CN129

The subcellular localisation of CN129 was investigated in living cells. For this purpose the human CFP-fusion proteins (see 3.7) were overexpressed in different cell lines (SH-SY5Y-, WT10-, Cos7- and HEK293 cells) and visualised by confocal laser scanning microscopy. CN129-CFP were found in cytosol and the nucleus throughout the cell, but was excluded from unidentified cellular structures in all tested cell lines. Counter-staining with DAPI (Fig. 3.17B) for nuclear visualisation did not provide evidence for exclusion from nucleoli. Overexpressed full length or partial CN129-CFP fusion proteins were not different in their cellular distribution. The exclusion pattern of CN129-CFP displayed similarities to structures observed in early apoptotic cells. However, cells were viable as cell and vesicle movement could be observed and the CN129-CFP distribution remained similar for > 1 h observation time. Overexpressed in SH-SY5Y, CN129-CFP was also found in axons and dendrites (Fig. 3.17 A, B).

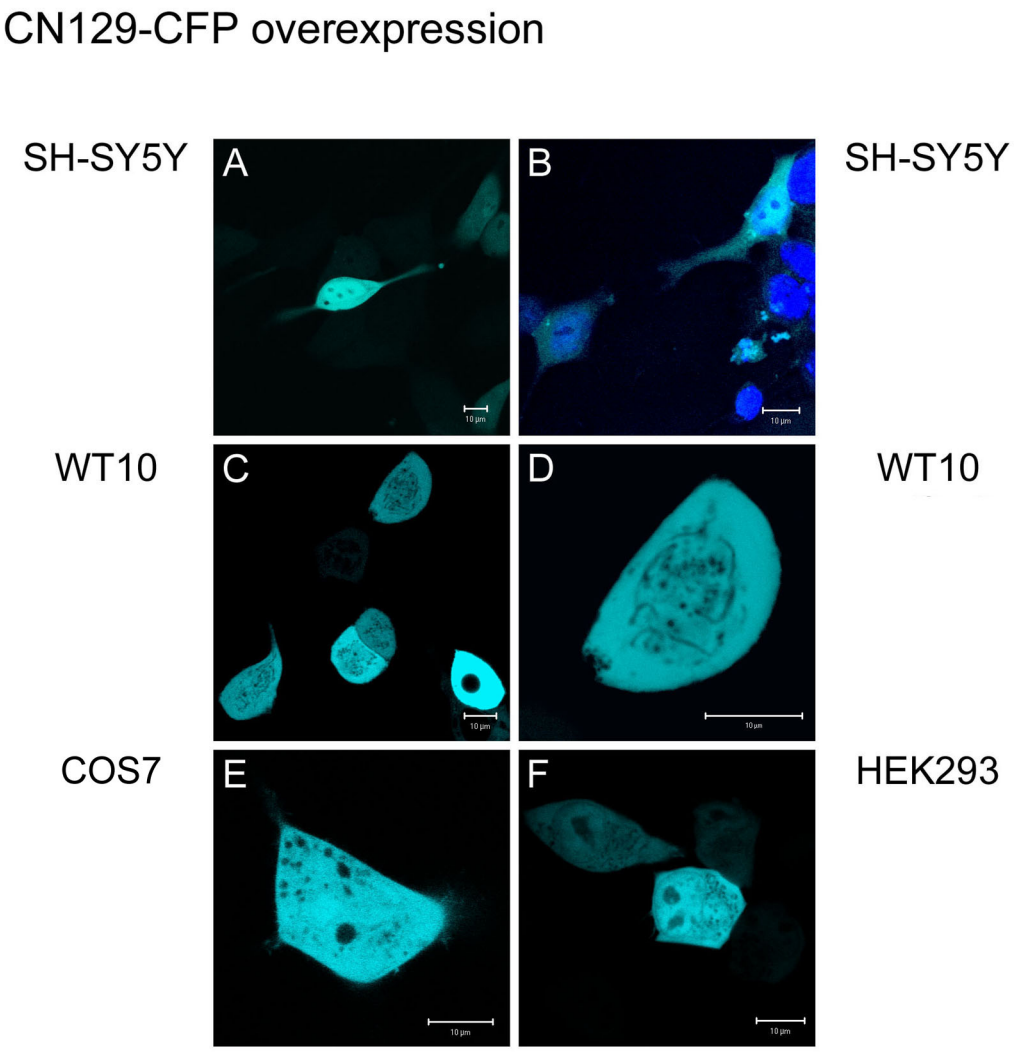

Figure 3.17: Subcellular distribution of CN129-CFP fusion protein in different cell lines. Full length human (C, D, F) or partial (A, B, E) CN129-CFP fusion protein was overexpressed in SH-SY5Y (A, B), WT10 (C; D), Cos7 (E) and HEK293 (F) cells. Living cells were analysed by confocal laser scanning microscopy. Cytoplasmatic and nuclear staining for CN129-CFP was observed throughout the cell. The CN129-CFP fusion protein was excluded from undefined subcellular structures. Counter-staining with a nuclear marker (DAPI, B) and magnification (D).

3.9 The CN129 protein is highly conserved

Bioinformatic analysis of CN129 showed that CN129 is a highly conserved protein. Searching the 'InterPro database' (http://www.ebi.ac.uk/interpro/; [125, 126]) resulted in the discovery of a 'domain of unknown function' DUF727 (IPR007967) spanning amino acids 22-134 and thereby covering almost the full length protein. This 'domain' is conserved within the *metazoa* and shows within the vertebrates a 68% amino acid identity between zebrafish (*D. rerio*) and human (*H. sapiens*) proteins. The conservation is shown in Fig. 3.18 A by taxonomic coverage and a multiple sequence alignment (derived from InterPro). To test whether the putative RII-binding domains of the members of the DUF727 family do bind to human RIIα subunits the cognate peptides were spot-synthesised and subjected to RII overlay assay. All but two peptides (*D. rerio*, *C. elegans*) bind to human RIIα subunits (for peptide sequences 2.1.3). The high degree of conservation implies that CN129 possesses an important cellular function common to vertebrates.

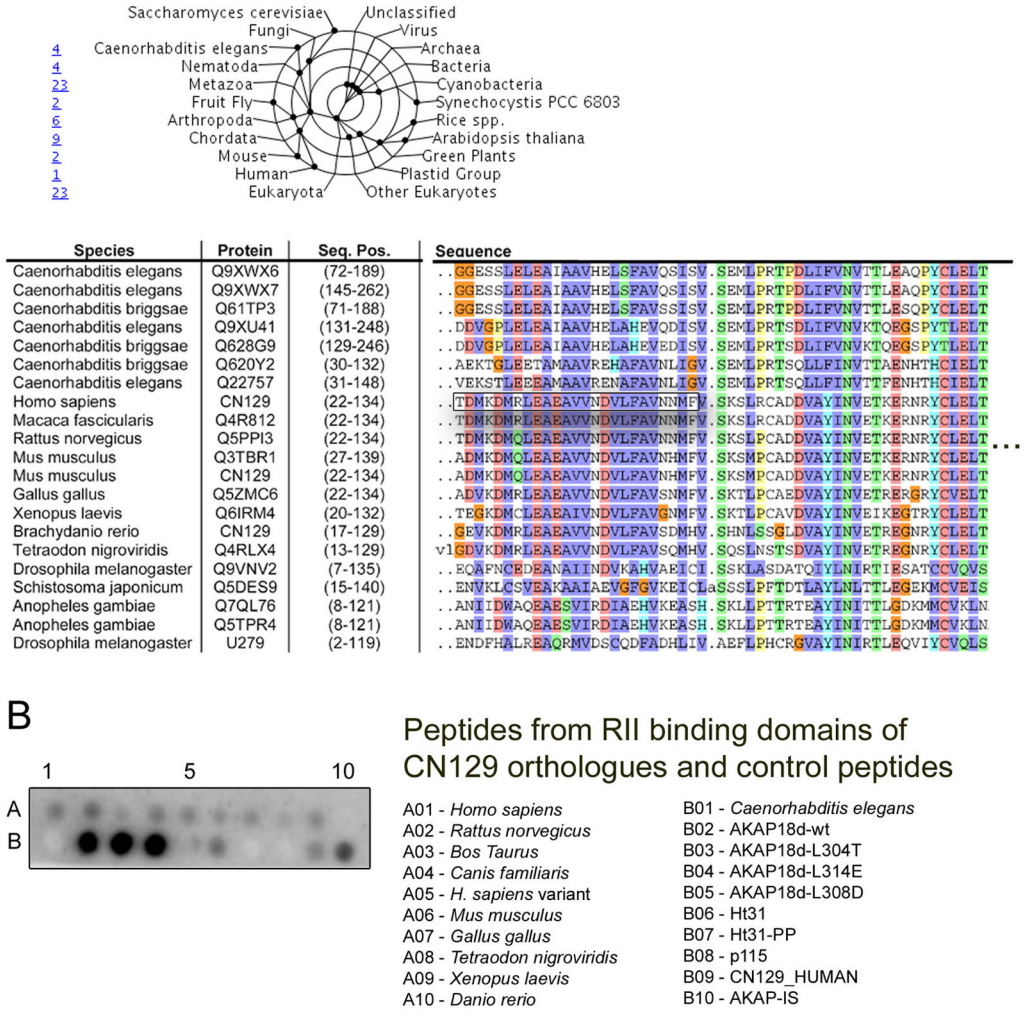

Figure 3.18: The amino acid sequence of human CN129 is highly conserved. A. Human CN129 is a member of a domain family annotated by similarity in the 'Interpro database' as domain of unknown function (DUF727, IPR007967). Shown is species distribution of this domain (upper panel) and a multiple sequence alignment of the cognate protein sequences (lower panel; species, swissprot protein id or accession number, sequence positions within the proteins and the N-terminal section of the alignment). The RII-binding domain of human CN129 is highlighted (black box). B. Peptides representing the putative RII-binding domains of the indicated members of the domain family and control peptides were spot-synthesised, assayed in RII overlay and analysed by autoradiography (note: the peptide sequences in positions A01 and B09 are identical).

3.10 The structure of the CN129 protein

The 'structure to function' analysis aims to elucidate function of proteins by comparative structural investigations. The Protein structure initiative, Northeast structural genomics consortium (NESG, www.nesg.org) picked human CN129 as representative member of the DUF727 family and determined its structure by NMR (pdb: 1sgo). CN129 is therefore the first AKAP whose structure is solved (Fig. 3.19). CN129 is composed of a 5-stranded, anti-parallel β-sheet and three α-helices, the N-terminal residues 1-31 form a unstructured coil. The RII-binding domain of CN129 (28-52) forms at the N-terminal amino acids 33-46 an α-helix as expected. Moreover, it runs *via* a turn into a short β-strand (50-54). The α-helix displays clearly an amphipathic character as the charged and polar amino acid residues (D32, R34, E36, E38, N42) are oriented on the opposite helical side as the hydrophobic amino acid residues in conserved positions (A37, V40, V41, V44, L45, V48). According to the NMR structure the latter, forming the contact surface to the RII dimer are masked by the anti-parallel β-sheet. Binding to RII subunits might therefore be coupled with major conformational changes of CN129. The electrostatic surface contains regions with two distinct properties. The CN129 structure shows an acidic patch which encompasses the β1 - β2 loop and the β3 - β4 loop. Conserved residues (see Fig. 3.18) cluster in this region and in a cleft spanning the central β-sheet, formed by connecting loops. CN129 additionally has an extended hydrophobic surface spanning the outer face of helix α3, where several conserved residues are present, suggesting a putative protein-protein interaction site. CN129 shows structural similarity to components of the Ubiquitin Conjugation Enzyme Complex as well as to the SH2 domain with differences in the β-strand organisation and the miss-

ing of the α3-helix (published on the NESG project progress summary web page, target-ID: HR969; http://spine.nesg.org).

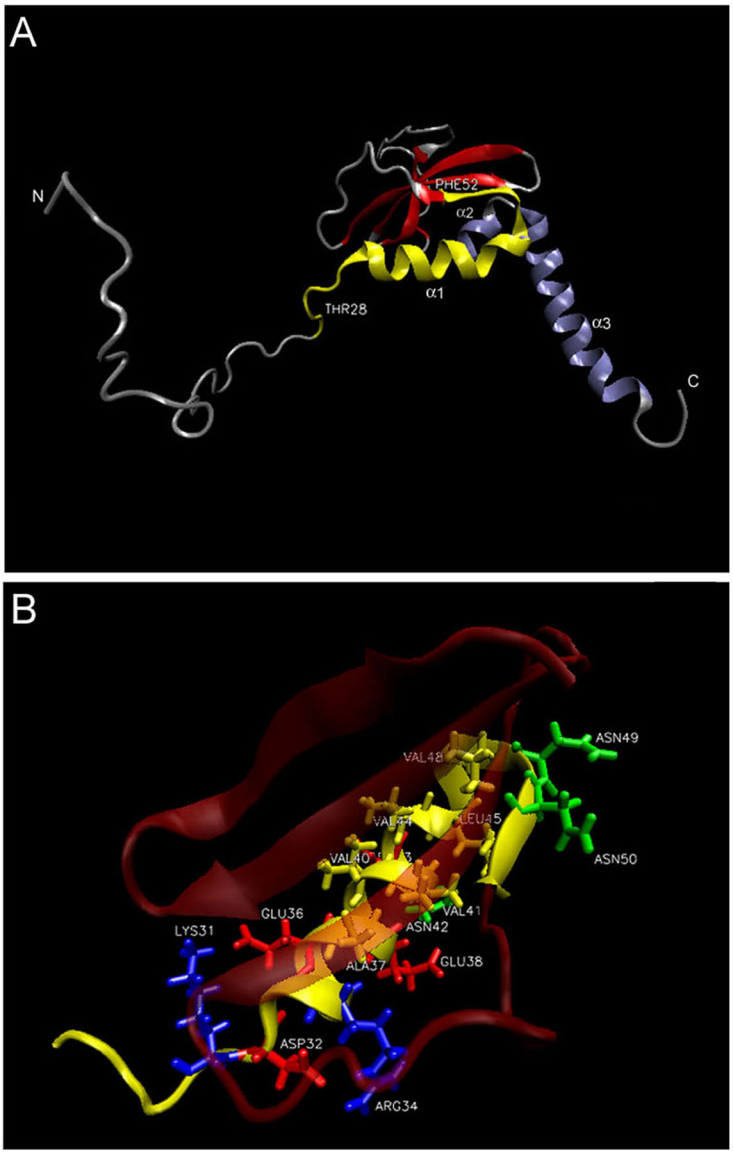

Figure 3.19: The NMR structure of the AKAP CN129. The NMR-structure of CN129 was solved by the Northeast structural genomics consortium (NESG, see text). A. CN129 is composed of a 5-stranded, anti-parallel β-sheet (red) and three alpha helices (α1; α2 and α3, blue). The RII-binding domain (highlighted in yellow) comprising amino acid residues 28-52 encompasses the α1-helix. The α3-helix is clearly exposed (N- and C-terminus as indicated). B. The RII-binding domain (yellow) encompasses the amphipathical α1-helix. Hydrophobic amino acid residues in conserved positions (yellow) and polar (green) or charged (negative: red, positive: blue) amino acid residues of the RII-binding domain are displayed. The expected contact face for RII-binding is shaded by the β-sheet (red).